

## New Internal-Charge-Transfer Second Order NLO Chromophores Based on the Donor Ferrocenylpyrazole Moiety

Kabali Senthilkumar, Maddalena Pizzotti, Krishnan Thirumoorthy, Gabriele Di Carlo,  
Stefania Righetto, Alessio Orbelli Biroli, Matti Haukka, and Nallasamy Palanisami

*J. Phys. Chem. C*, **Just Accepted Manuscript** • DOI: 10.1021/acs.jpcc.6b06364 • Publication Date (Web): 16 Aug 2016

Downloaded from <http://pubs.acs.org> on August 17, 2016

### Just Accepted

“Just Accepted” manuscripts have been peer-reviewed and accepted for publication. They are posted online prior to technical editing, formatting for publication and author proofing. The American Chemical Society provides “Just Accepted” as a free service to the research community to expedite the dissemination of scientific material as soon as possible after acceptance. “Just Accepted” manuscripts appear in full in PDF format accompanied by an HTML abstract. “Just Accepted” manuscripts have been fully peer reviewed, but should not be considered the official version of record. They are accessible to all readers and citable by the Digital Object Identifier (DOI®). “Just Accepted” is an optional service offered to authors. Therefore, the “Just Accepted” Web site may not include all articles that will be published in the journal. After a manuscript is technically edited and formatted, it will be removed from the “Just Accepted” Web site and published as an ASAP article. Note that technical editing may introduce minor changes to the manuscript text and/or graphics which could affect content, and all legal disclaimers and ethical guidelines that apply to the journal pertain. ACS cannot be held responsible for errors or consequences arising from the use of information contained in these “Just Accepted” manuscripts.

# New Internal-Charge-Transfer Second Order NLO Chromophores

## Based on the Donor Ferrocenylpyrazole Moiety

Kabali Senthilkumar,<sup>†</sup> Maddalena Pizzotti,<sup>‡\*</sup> Krishnan Thirumoorthy,<sup>†</sup> Gabriele Di Carlo,<sup>‡</sup> Stefania Righetto,<sup>‡</sup> Alessio Orbelli Biroli,<sup>§</sup> Matti Haukka,<sup>||</sup> Nallasamy Palanisami<sup>†\*</sup>

<sup>†</sup> Department of Chemistry, School of Advanced Sciences, VIT University, Vellore 632014, Tamil Nadu, India.

<sup>‡</sup> Department of Chemistry, University of Milan, INSTM Research Unit, Via C. Golgi 19, 20133 Milan, Italy.

<sup>§</sup> Istituto di Scienze e Tecnologie Molecolari del CNR (CNR-ISTM) Via C. Golgi 19, 20133 Milan, Italy

<sup>||</sup> Department of Chemistry, University of Jyväskylä, P.O. Box 35, FI-40014 Jyväskylä, Finland.

### Corresponding Authors

\*Nallasamy Palanisami: Email: [palanisami.n@gmail.com](mailto:palanisami.n@gmail.com); Tel: +91 9842639776

\*Maddalena Pizzotti: Email: [maddalena.pizzotti@unimi.it](mailto:maddalena.pizzotti@unimi.it); Tel: +39 0250314363

## Abstract

A series of new N-arylated ferrocenepyrazole structures, carrying different donor or acceptor substituents in the para position of the aryl ring has been synthesized by the Chan-Lam cross coupling reaction. The nonplanar geometric molecular structure of some of these chromophores together with their crystal packing was determined by X-ray diffraction and the HOMO and LUMO energy levels were evaluated by electrochemical and optical measurements and by DFT theoretical calculations. By the investigation of solvent effects and TD-DFT calculations the intense electronic absorption band at around 270-310 nm was confirmed to be an internal-charge-transfer (ICT) band, showing a significant red shift by increasing the electron withdrawing properties of the substituent on the para position of the aryl ring. TD-DFT calculations and EFISH measurements of the quadratic hyperpolarizability have shown that also the second order NLO response of these new ICT chromophores can be tuned by changing the nature of the substituent. Both theoretical  $\mu\beta$ ,  $\beta$  and experimental EFISH  $\mu\beta_{1907}$  and  $\beta_{1907}$  values are significant, with a quite satisfactory correlation of the general trend of theoretical  $\mu\beta$  and EFISH  $\mu\beta_{1907}$  values. The highest value of EFISH  $\mu\beta_{1907}$  ( $410 \times 10^{-48}$  esu) was measured for the chromophore carrying the strong electron withdrawing  $\text{NO}_2$  group.

## Introduction

Due to the potential applications in optical communications, data storage, field effect transistors, light emitting diodes, and dye-sensitized solar cells, molecular structures including electron-acceptor (A) and electron-donor (D) groups were extensively investigated as new functional materials.<sup>1-4</sup> Asymmetric organic or organometallic push-pull structures or molecular species characterised by internal-charge-transfer (ICT) processes, which have dipolar electronic structures, are potentially interesting nonlinear optical (NLO) molecular materials.<sup>5-7</sup> In particular examples of intramolecular charge-transfer<sup>8</sup> excitations, affording large dipole moment changes  $\Delta\mu_{eg}$  (difference between excited-state and ground-state dipole moments), as origin of significant quadratic hyperpolarizability ( $\beta$ ) and of quadratic electro-optic effect (QEO effect) have been reported.<sup>9-11</sup> Modulation of the charge-transfer processes in organometallic chromophores has provided excellent opportunities for tuning the second order nonlinear optical response,<sup>12-15</sup> so that push-pull and ICT organometallic chromophores based for instance on metals such as iron and ruthenium have been largely investigated.<sup>16</sup> Ferrocene has an ionization energy and redox electrochemical potentials comparable to those of the best organic donors,<sup>17</sup> together with a high chemical stability of both the neutral ( $\text{Fe}^{2+}$ ) and cationic ( $\text{Fe}^{3+}$ ) species with a facile interconversion between the two oxidation states.<sup>18</sup> Therefore, it has been investigated as an ideal organometallic donor building block for mixed-valence organometallic species,<sup>19</sup> magnetic charge-transfer,<sup>20</sup> photo-induced charge transfer,<sup>21</sup> and redox-active sensors for cations and anions detections.<sup>22</sup> Hence ferrocene, the first organometallic species reported as donor moiety for second-order NLO chromophores,<sup>15</sup> remains one of the most widely investigated donor species, comparable to N,N'-dimethyl, and methoxyphenyl organic donors. A significant series of investigations have been devoted to push-pull chromophores where the donor properties of ferrocene are due to the electronic coupling between the metal d-orbitals and the  $\pi$ -network of the donor-acceptor linker of the push-pull structure.<sup>17, 23-25</sup> [Second order NLO chromophores involving the ferrocenyl moiety as the donor](#)

part of an ICT process were investigated by some research groups, especially Qiu et al. but, still it need to be explore more.<sup>26-29</sup>

Pyrazoles are five-membered heterocyclic structures investigated as promising donor moieties for organic second-order NLO chromophores. Moreover, they may find applications in optical laser technology,<sup>30</sup> or as an electroluminescent source.<sup>31</sup> Blue emitting fluorescent dyes based on pyrazole structure characterized by high fluorescence quantum yield have been also reported.<sup>32</sup> Second order NLO properties of several pyrazole derivatives were investigated, showing relatively good  $\beta$  values.<sup>33-38</sup> For instance Miller et al.<sup>39</sup> have reported the first organic ICT chromophores based on an N-arylated pyrazolic structure, characterized by a quite good second order NLO response measured by EFISH technique. Moreover Zilio et al.<sup>40</sup> measured, by the HRS techniques, a  $\beta$  value of  $45 \pm 2 \times 10^{-30}$  esu for a second order NLO organic chromophore based on a substituted pyrazole. New pyrazole based push-pull second order NLO chromophores are reported to exhibit excellent values of ground state dipole moments and quadratic hyperpolarizability.<sup>41, 42</sup>

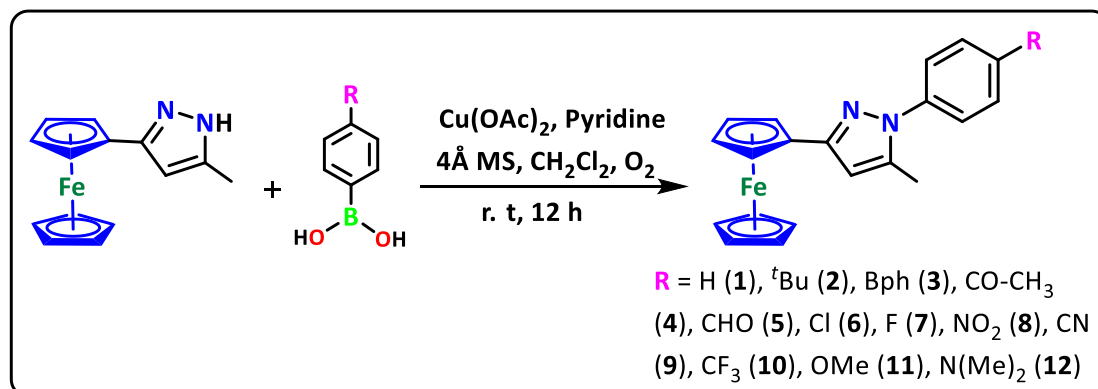
The present work focuses on the synthesis and on the structural, spectroscopic, electrochemical, theoretical and second order NLO characterization of ICT chromophores based on N-arylated ferrocenyl pyrazole derivatives [1-(4-R-phenyl)-5-methyl-3-ferrocenyl-1H-pyrazole (R = H, *tert*-butyl, Ph, CO(CH<sub>3</sub>), CHO, Cl, F, CF<sub>3</sub>, CN, NO<sub>2</sub>, OMe, NMe<sub>2</sub>)]. These chromophores have been synthesized by the Chan-Lam coupling reaction<sup>43, 44</sup> in good yields and characterized by microanalysis, FT-IR, FT-NMR and mass spectrometry. Their structures have been confirmed by single crystal X-ray diffraction (XRD) and their electronic absorption spectra and electrochemical properties have been experimentally investigated and theoretically analyzed by DFT and TD-DFT methods. Their second order NLO responses were experimentally measured by means of the EFISH technique and theoretically calculated by the TD-DFT approach.

## Results and Discussion

### Synthesis, physicochemical and crystallographic characterization

The starting material [3-ferrocenyl-5-methyl-1H-pyrazole] was prepared by reaction of a ferrocenyl  $\beta$ -diketone (FcCOCHCOCH<sub>3</sub>)<sup>45</sup> with hydrazine hydrate (1:1 ratio) according to the literature.<sup>46</sup> Many synthetic routes for the synthesis of N-arylated pyrazole derivatives involve the condensation of N-arylated hydrazine with the  $\beta$ -diketone moiety, while alternative routes involving a C-N coupling reaction were developed by using NaH,<sup>47</sup> Cs<sub>2</sub>CO<sub>3</sub> and K<sub>2</sub>CO<sub>3</sub> based Cu catalysts<sup>48, 49</sup> and Zn-Li<sup>50</sup> based catalysts. However, our attempts to synthesize by these routes N-arylated ferrocenyl pyrazoles were unsuccessful. Therefore, we synthesized these molecules following the Chan-Lam coupling reaction<sup>43, 44</sup> which is a copper salt-promoted cross coupling (scheme 1). The reaction proceeds under relatively mild conditions independently from the nature of the substituents on the phenyl ring. [A possible reaction mechanism is reported in scheme S1](#) while details are given in the Supporting Information. The Chan-Lam coupling reaction proceeds stereo and regioselectively with excellent yields by copper catalyzed N-arylation of ferrocenyl-5-methyl-1H-pyrazole. The products [1-(4-R-phenyl)-5-methyl-3-ferrocenyl-1H-pyrazole (R = H, *tert*-butyl, Ph, COCH<sub>3</sub>, CHO, Cl, F, CF<sub>3</sub>, CN, NO<sub>2</sub>, OMe, NMe<sub>2</sub>) were obtained by reaction of [3-ferrocenyl-5-methyl-1H-pyrazole] in CH<sub>2</sub>Cl<sub>2</sub> solution with various arylboronic acids in the presence of copper<sup>II</sup> acetate, pyridine and 4Å molecular sieves (see supporting Information). All the chromophores were unambiguously characterized by FT-IR, FT-NMR and Electron Ionization (EI)-mass spectroscopies. The pyrazole moiety could allow the formation of regioisomers, but for all the chromophores investigated (**1-12**) (see Scheme 1) one major regioisomer was predominant. The minor regioisomer produced in low yield (<5%), was easily separated by column chromatography. The thermogravimetric analysis confirmed a thermal stability in the air up to 300 °C (see TGA of **8** and **9** reported in Figure S1), so that all the chromophores could be stored without special precautions. The structures of

chromophores **5**, **7**, **8** and **9** were fully characterized by single crystal X-ray diffraction (Table S1 and Figure 1) and by  $^1\text{H}$  NMR spectroscopy.



**Scheme 1.** The Chan-Lam synthesis of chromophores **1-12**.

The C-N coupling bond formation for chromophores **5**, **7**, **8** and **9** at the desired nitrogen atom was confirmed by crystals grown by recrystallization from different mixed solvents (CH<sub>3</sub>OH, CHCl<sub>3</sub>, and CH<sub>2</sub>Cl<sub>2</sub>) at room temperature. The structures of **5**, **7**, **8** and **9** are shown in Figure 1 with the appropriate atom numbering. The data collections, structure refinement as well as the parametric data of the unit cells are given in Table S1, whereas Table 1 contains the most relevant bond lengths, bond angles and dihedral angles for **5**, **7**, **8** and **9**. All the chromophores crystallize in the centrosymmetric space groups (**5**, **7** and **9**: monoclinic P lattice with P2<sub>1</sub>/c; **8**: monoclinic P lattice with P2<sub>1</sub>/n), thus, they are not expected to show any bulk nonlinear optical property.<sup>51, 52</sup>

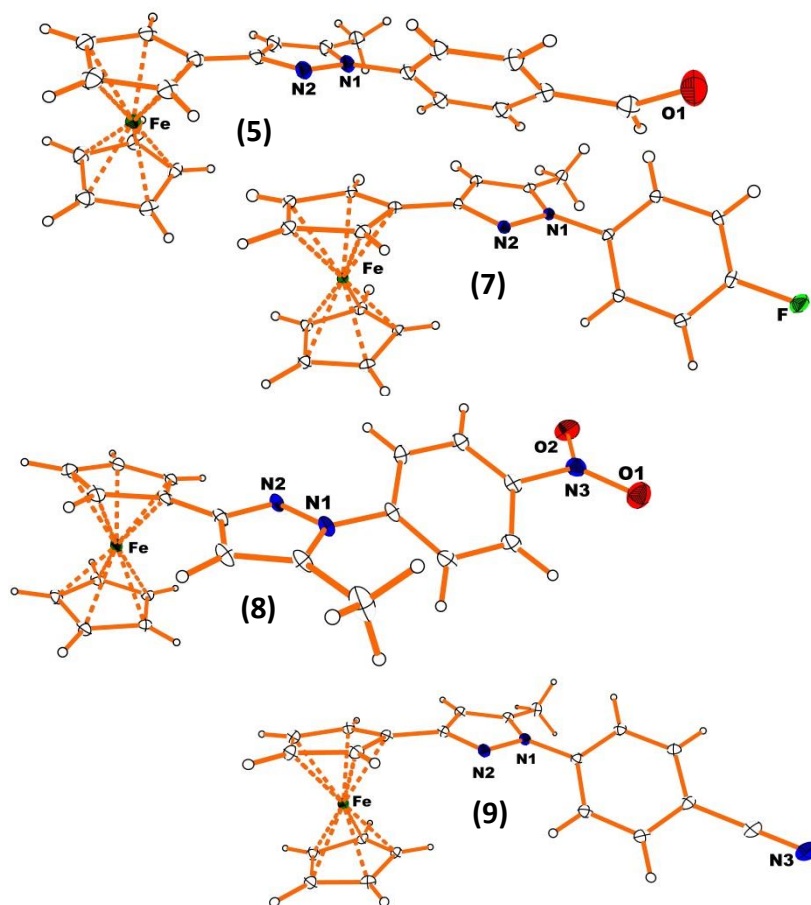


**Figure 1.** Representation of the crystallographic molecular structure of chromophores **5**, **7**, **8** and **9** (with 30% probability ellipsoids), with numbering of C, N, O, F and Fe atoms.

The crystal packing of chromophores **5**, **7-9** shows the antiparallel alignment of the neighboring chromophores; the overlap pictograms of the aromatic rings and other inter and intra-atomic interactions are shown in Figures S2-S7 and exhibit inter and intramolecular interactions *via* hydrogen bonding and  $\pi\cdots\pi$  interactions. For instance **5** shows a hydrogen bonding network *via* C-H $\cdots$ O contacts particularly stabilized by  $\pi\cdots\pi$  (3.362 Å) and C-H $\cdots\pi$  (3.385 Å) interactions involving the cyclopentadienyl ring as shown in (Figure S3), while **7** shows strong H-F bonding of 2.455 and 2.961 Å between two adjacent rings, with a stabilisation of a sheet-like structure (Figure 2).



The geometric parameters of all the chromophores are closely related<sup>53, 54</sup> and characterized by a slight twist angle between the cyclopentadienyl ring of ferrocenyl and the pyrazole ring, and with a torsion angle between the pyrazole and the aromatic rings. It follows that the arrangement of the total  $\pi$  structure is not planar, although the arrangement between the cyclopentadienyl ring of the ferrocenyl and the pyrazole moieties is slightly planar (Figure 3). As shown in Figure 3 the lack of planarity of the structures of **5**, **7-9** is measured by their cyclopentadienyl-pyrazole twist angle and by their torsion or dihedral angles  $\phi_1$  and  $\phi_2$  between the ferrocenylpyrazole moieties and the substituted phenyl ring respectively.

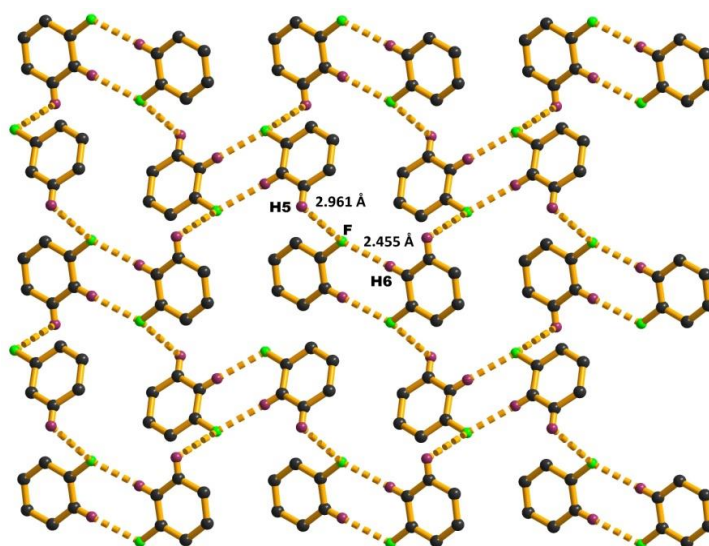


**Figure 2.** Core sheet-like formation by H $\cdots$ F bonding in the crystal structure of **7**, with H $\cdots$ F hydrogen bond distances of 2.455 and 2.961 Å.

A pictorial representation of the values (given in Table 1) of  $\phi_1$  and  $\phi_2$  is reported in Figure S8. The torsion between the plane of the pyrazole and the phenyl ring reduces the  $\pi$  interaction and therefore the intramolecular charge-transfer process which should control the molecular second-order NLO response.<sup>55</sup> As reported in Table 1 the values of angles  $\phi_1$  and  $\phi_2$  indicate that the aromatic and pyrazole rings are quite twisted in all the chromophores as confirmed by DFT optimized structures of **1**, **7-12** reported in Figure S9.

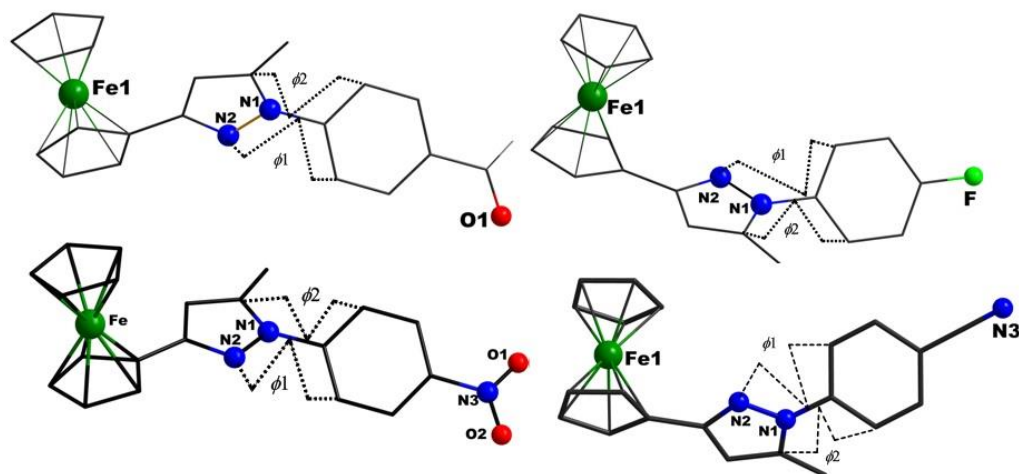


**Figure 3.** Dihedral or torsion angle  $\phi_1$  and  $\phi_2$  of **5**, **7**, **8** and **9**.

**Table 1.** Relevant structural parameters of **5**, **7**, **8** and **9**. The interatomic distances are reported in Å, angles in degrees.

Chromophore	<b>5</b>	<b>7</b>	<b>8</b>	<b>9</b>
Average Fe-C	2.052(4)	2.046(9)	2.049(9)	2.046(2)
Fe-Cent(1)	1.655(5)	1.648(0)	1.650(2)	1.648(3)
Fe-Cent(2)	1.651(5)	1.646(2)	1.653(4)	1.646(0)
Cent(1)-Fe(1)-Cent(2)	177.72(3)	178.95(9)	178.35(8)	179.22(8)
N(1)-N(2)	1.370(9)	1.370(3)	1.372(7)	1.371(3)
N(1)-C(8)	1.372(1)	1.368(2)	1.373(8)	1.370(2)
N(1)-C(5)	1.416(1)	1.422(5)	1.413(3)	1.408(8)
N(2)-C(11)	1.335(1)	1.338(6)	1.331(6)	1.333(8)
C(11)-C(12)-N(1)	157.89(3)	160.16(0)	158.27(5)	160.22(5)
C(11)-N(1)-C(5)	155.45(1)	157.58(0)	155.37(7)	155.71(5)
N(1)-C(5)-C(1)	178.31(5)	178.71(3)	177.49(2)	178.58(1)
Cp-pyrazole twist angle	-14.93	8.74	-11.17	-13.16
N(2)-N(1)-C(4)-C(5) $\phi_1$	-45.37	46.92	-42.92	-42.75
C(7)-N(1)-C(4)-C(3) $\phi_2$	-38.22	51.47	-33.56	-34.06

## Electrochemical Studies

Electrochemical potentials for second order NLO chromophores provide required information about HOMO and LUMO energy levels.<sup>56</sup> Therefore, we have carried out cyclic voltammetry (CV) measurements at 0.2 Vs<sup>-1</sup> on a glassy carbon working electrode in acetonitrile solution with 0.1 M tetrabutylammonium perchlorate (TBAP) as the supporting electrolyte. A saturated calomel electrode (SCE) was used as the operating reference electrode and a platinum

wire as the counter electrode. The electrochemical data of the oxidation and reduction processes of the chromophores **1**, **7-12** are reported in Table 2, and the representative cyclic voltammograms of **2**, **8**, **9** and **10** are shown in Figure S10. All the chromophores display the first oxidation peak reversible or quasi-reversible from both the electrochemical and chemical point of view with a current ratio ( $i_{pa}/i_{pc}$ ) equal to unity, assignable to the monoelectronic oxidation process of the ferrocenyl ( $Fe^{II} \leftrightarrow Fe^{III}$ ) moiety within the potential range of +0.44 to +0.36 V. Compared to 0.40 V of the oxidation potential of the free ferrocene in the same experimental conditions,<sup>57</sup> the chromophores **8**, **9** and **10** exhibit slightly higher oxidation potentials, while the chromophores **1**, **7**, **11** and **12** show slightly lower potentials.<sup>58</sup>

However, the peak corresponding to the reduction could be detected only for chromophores **8**, **9**, **10** (Table 2 and Figure S10), carrying electron withdrawing groups in a *para* position of the aryl ring. The reduction potential of aromatic moiety of the chromophores **1**, **2**, **7**, **11** and **12** could not be detected in the working potential window, as clearly shown in Figure S10 for **2** taken as an example. This can be explained by the significant effect produced on the reduction potential by the electron withdrawing properties of the substituent in the *para* position. In fact the potential of the reduction process shifts significantly from -1.79 V (**8**) to -2.17 V (**9**) and -2.39 V (**10**) as expected for a more easy process by increasing the electron withdrawing properties of the substituent in the *para* position of the aromatic ring.

Therefore, it appears that the potential of the oxidation process, which is centered on the ferrocenyl moiety, is only slightly affected by the electronic effects induced by the substituent, while the potential of the reduction process, which is centered on the aromatic ring, is significantly affected. It follows that the energy of electrochemical HOMO level is quite comparable for all the chromophores while the energy of the electrochemical LUMO level is higher for **9** and **10** when compared to **8** and probably much higher for **1**, **7** and particularly for **11** and **12**. Any attempt to evaluate the energy of the LUMO levels of **1**, **7**, **11** and **12** by the electrochemical and optical

method ( $E_{\text{LUMO}} = E_{\text{HOMO}} + E_{\text{g}}^{\text{optical}}$  where  $E_{\text{g}}^{\text{optical}} = 1239.84187/\lambda_{\text{onset}}$ ) failed, due to the very weak intensity and broad characteristic of their low-energy absorption band, which introduces a great difficulty in defining the value of  $\lambda_{\text{onset}}$  without introducing large errors.

**Table 2.** Key CV features of chromophores **1**, **7-12** and electrochemical energy levels HOMO and LUMO derived therefrom.

Chromophore	$E_{1/2,\text{lc}}$ [V]	$E_{1/2,\text{la}}$ [V]	$E_{\text{LUMO}}$ [eV] <sup>b</sup>	$E_{\text{HOMO}}$ [eV] <sup>c</sup>	$E_{\text{HOMO-LUMO}}$ [eV]
<b>1</b>	n.d.	0.38	n.d.	-4.78	n.d.
<b>7</b>	n.d.	0.37	n.d.	-4.77	n.d.
<b>8<sup>a</sup></b>	-1.79	0.41	-2.66	-4.81	2.15
<b>9</b>	-2.17	0.44	-2.23	-4.84	2.61
<b>10</b>	-2.39	0.44	-2.01	-4.84	2.83
<b>11</b>	n.d.	0.36	n.d.	-4.76	n.d.
<b>12</b>	n.d.	0.37	n.d.	-4.77	n.d.

a) A reduction peak is detected at -1.05 V, corresponding to the reduction of the nitro group (see Figure S10)

b)  $E_{\text{LUMO}} = -(E_{1/2,\text{lc}} + 4.4)$  c)  $E_{\text{HOMO}} = -(E_{1/2,\text{la}} + 4.4)$  (n.d.= not detected).

## Electronic absorption spectra

The absorption spectra of the chromophores **1** and **7-12** in  $\text{CH}_3\text{CN}$  solution are shown in Figure 4a, and HE (high energy), ME (medium energy) and LE (low energy) absorption bands of chromophores **9** and **10** in Figure 4b, while detailed data about the absorption maxima of chromophores **1** and **7-12** are reported in Table 3. All the chromophores depict an intense absorption band in the range 264-320 nm (HE), and a less intense band which sometimes, as in the case of **8**, **11** and **12** is a barely distinguishable shoulder in the region 335-380 nm (ME). Finally, all the chromophores show a very weak absorption band at about 440-460 nm (LE) only slightly dependent upon the nature of the substituent in the *para* position of the aryl ring (Table 3).

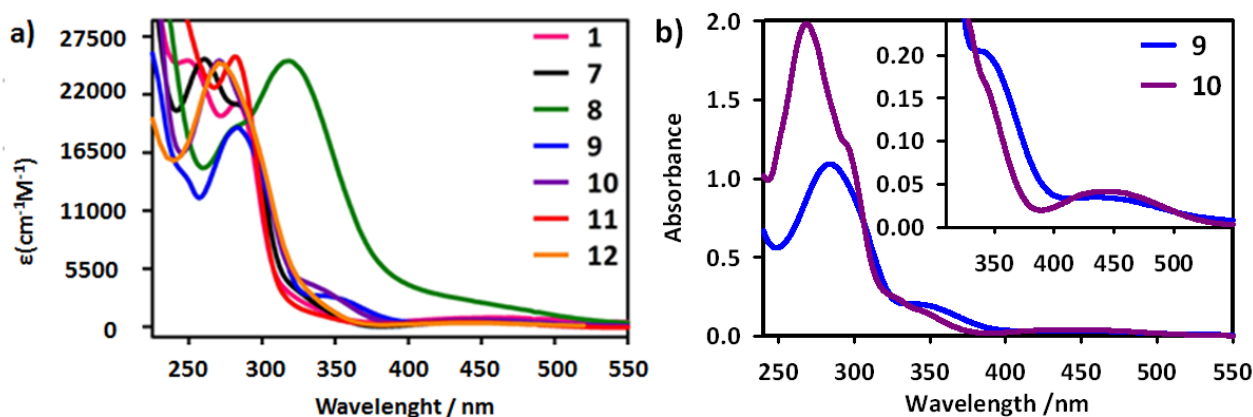


**Figure 4.** a) Electronic absorption spectra of chromophores **1** and **7-12**. b) HE, ME and LE absorption bands of **9** and **10** in CH<sub>3</sub>CN solution.

The HE band can be originated mainly from the N-arylpyrazolic moiety of the chromophores; for instance such very strong absorption band was reported for various N-arylpyrazoles by Miller *et al.*<sup>39</sup> The maximum of the HE band for all the chromophores investigated in this work, with the exception of **8**, is shifted to lower wavelengths with respect to the strong absorption band above 310 nm reported for various N-arylpyrazoles.<sup>39</sup> In agreement with such assignment for 3,5 dimethyl 1-(4-nitrophenyl)-1H pyrazole a strong band with  $\lambda_{\max}$  at 311 nm and  $\epsilon = 11748 \text{ M}^{-1} \text{ cm}^{-1}$  was reported by D.M. Burness.<sup>59</sup>

**Table 3.** Experimental data of the HE, ME and LE absorption bands of **1**, **7-12** in CH<sub>3</sub>CN solution.

Chromophore	$\lambda_{\max}^{\text{HE}}$	$\lambda_{\max}^{\text{ME}}$	$\lambda_{\max}^{\text{LE}}$
	[nm (eV)]/ $\epsilon (\times 10^3)$ [M <sup>-1</sup> cm <sup>-1</sup> ]	[nm (eV)]/ $\epsilon (\times 10^3)$ [M <sup>-1</sup> cm <sup>-1</sup> ]	[nm (eV)]/ $\epsilon (\times 10^3)$ [M <sup>-1</sup> cm <sup>-1</sup> ]
<b>1</b>	276 (4.48) /21.5	335(3.70)/1.85	449(2.76)/0.81
<b>7</b>	275 (4.50) /22.9	334(3.71)/2.61	440(2.81)/0.43
<b>8</b>	318 (3.89) /24.8	382(3.24)/6.40 <sup>a</sup>	460(2.69)/1.71 <sup>a</sup>
<b>9</b>	285 (4.36) /18.3	351(3.53)/2.79	450(2.75)/0.42
<b>10</b>	264 (4.69) /24.5	343(3.61)/3.32	446(2.77)/0.61
<b>11</b>	276 (4.49) /25.2	335(3.70)/1.27 <sup>a</sup>	440(2.81)/0.43
<b>12</b>	270 (4.59) /25.1	337(3.67)/2.13 <sup>a</sup>	445(2.78)/0.41

a) Barely distinguishable shoulder

1  
2  
3 The HE band of chromophores **1**, **7-12**, like the strong absorption band reported for various  
4 N-arylpyrazoles,<sup>39</sup> is not significantly solvatochromic, while its energy is controlled by the nature of  
5 the substituent with a strong or significant bathochromic shift for chromophores **8** and **9** carrying  
6 stronger electron acceptor groups in para position of the aromatic ring. Taking as reference  
7 chromophore **1** the HE band of **8** is red shifted by 42 nm while that of **9** by 9 nm, in agreement with  
8 the increased electron withdrawing character of the NO<sub>2</sub> group when compared to the CN group.  
9 Conversely, chromophores **11** and **12**, carrying respectively the slightly donor group OCH<sub>3</sub> and the  
10 strong donor group NMe<sub>2</sub>, show a very small or null hypsochromic shift when compared to **1** (Table  
11 3). It appears thus that the electronic effects produced by the substituents in the *para* position of the  
12 aromatic ring are transmitted along the entire molecular skeleton, although the  $\pi$   
13 ferrocenylpyrazolic moiety is not coplanar with the aromatic ring.  
14  
15  
16  
17  
18  
19  
20  
21  
22  
23  
24  
25  
26  
27  
28  
29

30 This statement is supported by the evidence that 3-ferrocenyl-5-methyl-1H-pyrazole, lacking  
31 the aryl ring, shows a strong absorption band in CH<sub>3</sub>CN solution at 270 nm ( $\epsilon = 32125 \text{ M}^{-1}\text{cm}^{-1}$ ),  
32 blue-shifted with respect to the HE band of all the other chromophores here investigated, with the  
33 exception of **12**, (Table 3). The ME and LE absorption bands of our chromophores seem to be  
34 originated mainly by the ferrocenyl moiety since substituted ferrocenyl molecules are characterized  
35 by three absorption bands.<sup>60</sup> The one at a shortest wavelength in the range of 269-289 nm of  
36 medium intensity ( $\epsilon$  about  $3000 \text{ M}^{-1}\text{cm}^{-1}$ ), is probably part of the strong HE band of **1**, **7-12**.  
37  
38  
39  
40  
41  
42  
43  
44  
45  
46  
47

48 The ME band of chromophores **1**, **7-12** (in the range 335-382 nm) can be attributed mainly  
49 to a MLCT transition centered on the ferrocenyl system and perturbed by its coupling with N-  
50 arylpyrazole and originated, according to Rabie,<sup>60</sup> by a  $n \rightarrow \pi^*$  transition from the Fe<sup>II</sup> atom to the  
51 cyclopentadienyl ring. This interpretation is supported by a significant red shift of the ME band for  
52 **8**, **9**, **10** and an increase in its intensity (Table 3), with respect to that of the 3-ferrocenyl-5-methyl-  
53 1-H-pyrazole ( $\lambda_{\text{max}}$  at 335 nm with  $\epsilon = 1400$ ), lacking the aryl ring. The LE band can be attributed  
54 to a very weak absorption at about 440 nm ( $\epsilon$  around  $460\text{-}590 \text{ M}^{-1}\text{cm}^{-1}$ ), typical of the ferrocenyl  
55  
56  
57  
58  
59  
60

1  
2  
3 moiety assigned, according to Rabie,<sup>60</sup> to a d-d transition within the d<sup>6</sup> iron atom. In accordance, the  
4 energy of this band is not too much dependent by the nature of the substituent in para position of the  
5 aryl ring (Table 3).  
6  
7  
8  
9

10  
11 It appears thus that despite the lack of planarity of the structure of chromophores **1**, **7-12** a  
12 significant electronic effect is transmitted on the energy and intensity of the MLCT transition of the  
13 ferrocenyl moiety according to the electronic nature of the substituent. For instance when  
14 comparing chromophore **1** with **8** and **9**, carrying the electron withdrawing groups NO<sub>2</sub> and CN in  
15 para position of the aryl ring, the ME band shows a bathochromic shift of 47 nm for **8** and 16 nm  
16 for **9** (Table 3), as expected if the ferrocenyl moiety, when linked to an N-arylpirazole, significantly  
17 participates to an ICT process.  
18  
19  
20  
21  
22  
23  
24  
25  
26  
27

28 Finally, the LE band of chromophores investigated in this work is not solvatochromic and  
29 very slightly perturbed as energy by the nature of the substituent, with an exception for **8**, carrying  
30 the strong electron withdrawing NO<sub>2</sub> group (Table 3). Such evidence suggests the assignment of  
31 this band to a d-d transition centered mainly on the ferrocenyl moiety, not much perturbed by the  
32 coupling between the cyclopentadienyl ring and the N-arylpirazole. In conclusion, the electronic  
33 absorption spectra of the chromophores support an ICT process despite the lack of planarity of their  
34 structures.  
35  
36  
37  
38  
39  
40  
41  
42  
43  
44

#### 45 **DFT and TD-DFT calculations**

46  
47  
48  
49 In order to find a solid theoretical support to the electronic origin of the ICT process, and  
50 consequently the main features of the electronic absorption spectra and of the second order NLO  
51 response, B3LYP/6-31+G\*\* and TD (B3LYP/6-31+G\*\*) calculations both in gas phase and in  
52 solvent (CH<sub>3</sub>CN) phase were carried out for chromophores **1** and **7-12**. The DFT optimized  
53 molecular structures of **1** and **7-12**, reported in the Supplementary Information (Figure S9), are  
54 totally in agreement with the main features of the structures deduced from the X- ray  
55  
56  
57  
58  
59  
60

crystallographic investigation of **5**, **7**, **8** and **9**. As it can be deduced from the isodensity plots of Figure 5, reporting also the energy of the HOMO and LUMO levels of **1**, **7-12**, the energy of the HOMO level, in agreement with the electrochemical investigation, is not too much influenced by the nature of the substituent in para position of the aromatic ring since the electronic density in the ground state is mainly localized on the ferrocenyl moiety. On the contrary, the energy of the LUMO level is strongly influenced by the substituent, as supported by the electrochemical investigation in the case of **8**, **9** and **10**, being the LUMO principally localized on the aromatic ring.

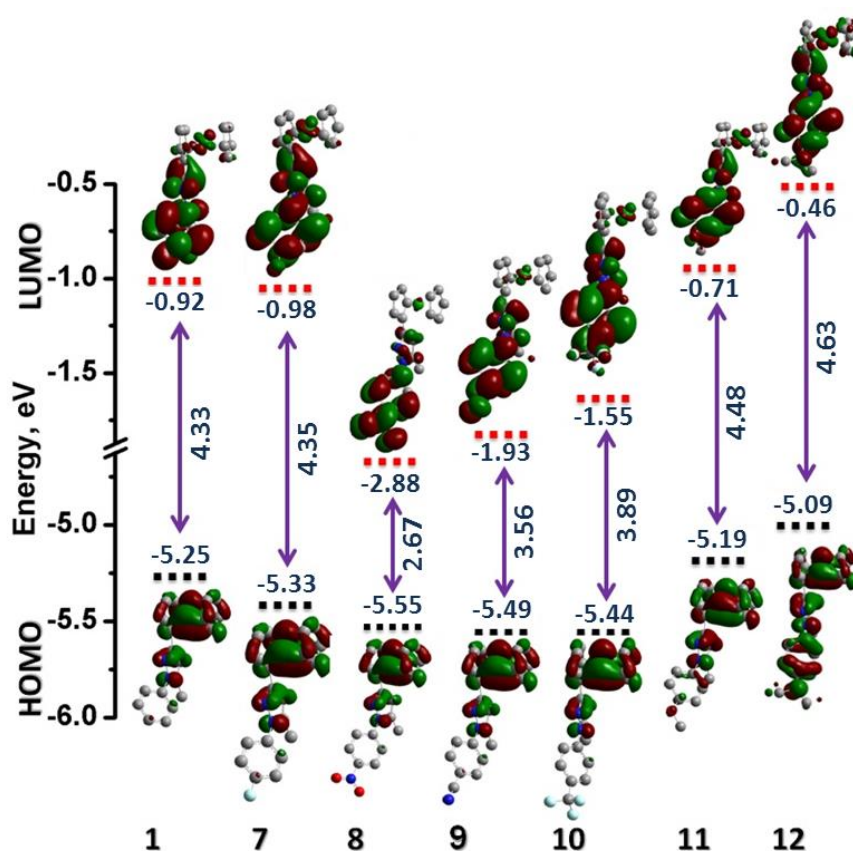


**Figure 5.** Isodensity plots, energy of the HOMO and LUMO levels and the HOMO-LUMO energy gap of chromophores **1** and **7-12** calculated at the B3LYP/6-31+G\*\* level of theory.

Only in the case of **12**, carrying a strong donor NMe<sub>2</sub> group in a *para* position of the aromatic ring, the HOMO has partially delocalized also on the aromatic ring and the LUMO on the ferrocenyl moiety. In detail the energy of the HOMO level shows, in agreement with the electrochemical trend, only a slight energy stabilization for **7**, **8**, **9** and **10**, and a slight



1  
2  
3 destabilization for **11** and **12**, when compared to **1** (Figure 5). DFT calculated values of the HOMO  
4 energy levels, ranging from about -5 to -5.5 eV, are lower than those deduced from the oxidation  
5 peaks of the electrochemical investigation (compare Figure 5 and Table 2), which are at about -  
6  
7  
8  
9  
10 4.75/-4.85 eV.

11  
12  
13 The energy of the LUMO level shows, when compared to **1**, a strong stabilization for **8**,  
14 carrying the strong electron withdrawing NO<sub>2</sub> group and a significant stabilization for **9** and **10**,  
15 carrying less strong electron acceptor groups, while a significant destabilization occurs for **11** and  
16  
17  
18  
19  
20  
21  
22 **12** carrying the electron donor OCH<sub>3</sub> and NMe<sub>2</sub> groups. Such trend reproduces quite well that  
23 deduced from the electrochemical investigation for **8**, **9** and **10** (Table 2). As found for the HOMO  
24 levels, the LUMO energy levels, with the exception of **8**, are higher than those deduced from the  
25 electrochemical investigation. As a result higher energy gaps are obtained with respect to the  
26  
27  
28  
29  
30  
31  
32  
33  
34  
35  
36  
37  
38  
39  
40  
41  
42  
43  
44  
45  
46  
47  
48  
49  
50  
51  
52  
53  
54  
55  
56  
57  
58  
59  
60  
electrochemical values (compare Figure 5 and Table 2) though the computed trend properly  
reproduces the experimental one. In particular for chromophores **8-10**, carrying electron  
withdrawing groups on the aromatic ring, the DFT calculated HOMO-LUMO energy gap increases  
from 2.67 eV to 3.56 and 3.89 eV respectively, while the electrochemical energy gap goes from  
2.16 eV to 2.61 and 2.83 eV respectively. The disagreement between computed and experimental  
values can be ascribed on one side to the adopted computational approach and, on the other side, to  
the effects of solvation and ionic couples which affect the electrochemical values of both the  
HOMO and LUMO energy levels.

By looking at the frontier orbital distributions of Figure 5, it turns out that the HOMO-  
LUMO transition corresponds, for **1**, **7-11**, to a large transfer of electron density from the ferrocenyl  
moiety to the N-arylpyrazolic system and particularly to the aromatic ring, while such electron  
transfer is not so significant for **12**. The role of the pyrazolic part of the molecule is not only that of  
allowing the transfer of the electronic density from the ferrocenyl to the aromatic ring but also of  
electron donor by a partial transfer of its electronic density to the aromatic ring.

We have then made TD-DFT calculations on chromophores **1** and **7-12** to give a definite assignment of the transitions experimentally observed (Table 4). They have confirmed the significant experimental red shift of the HE band by increasing the electron acceptor properties of the substituent in the *para* position of the aromatic ring and the ICT character of such band. A quite satisfactory agreement between calculated (Table 4) and experimental (Table 3) values of  $\lambda_{\max}$  of the HE band was found for **1** and **7**, **11** and **12**, while for chromophores **9**, **10** and particularly **8**, carrying strong electron acceptor groups, the difference between calculated and experimental values of  $\lambda_{\max}$  of the HE band is relevant.

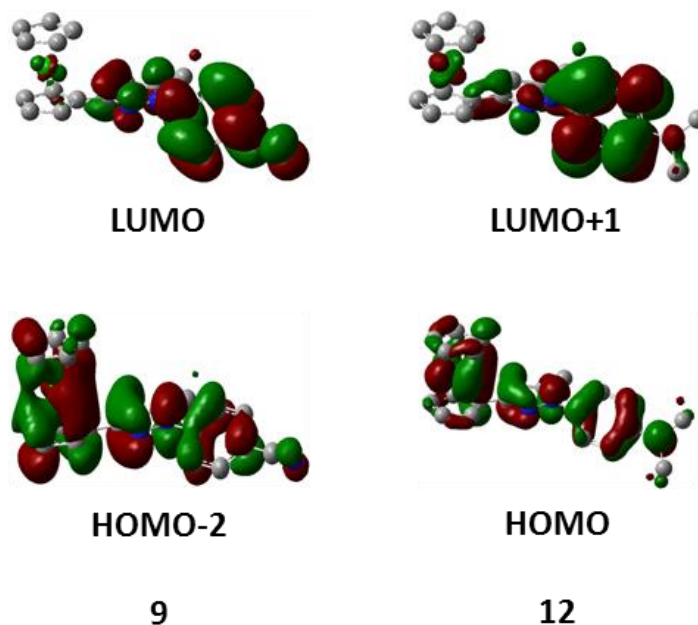
The anomaly of chromophore **8** is confirmed by the definition of the various relevant components of the HE band. While for **7**, **9**, **10**, **11** the major component is the HOMO-2  $\rightarrow$  LUMO transition, for **8** it is the HOMO-2 $\rightarrow$ LUMO+5. It appears that when the substituent can interact by conjugation with the  $\pi$  system of the aromatic ring like in **8** (Figure S11), but also in **12** carrying the strong donor NMe<sub>2</sub> group in the aryl ring (HOMO $\rightarrow$ LUMO+1 as the major component) there is an effect on the energy levels strongly involving the substituent by conjugation.

**Table 4.** TD-DFT calculated  $\lambda_{\max}$ ,  $f$  and energy contribution to the HE band at the major B3LYP/6-31+G\*\* level of theory for **1**, **7-12**

Chromophore	TD-DFT calculated $\lambda_{\max}$ and main features of the various relevant components to the HE band			
	$\lambda_{\max}$ , nm <sup>a</sup>	$f^a$	Energy, eV <sup>a</sup>	main transition (weight) <sup>b</sup>
<b>1</b>	280 (280)	0.19 (0.42)	4.43 (4.42)	HOMO-5 $\rightarrow$ LUMO (50%)
<b>7</b>	278 (279)	0.26 (0.41)	4.45 (4.44)	HOMO-2 $\rightarrow$ LUMO (+62%)
<b>8</b>	404 (449)	0.20 (0.25)	3.07 (2.76)	HOMO-2 $\rightarrow$ LUMO+5 (68%)
<b>9</b>	322 (329)	0.36 (0.46)	3.85 (3.76)	HOMO-2 $\rightarrow$ LUMO (+100%)
<b>10</b>	301 (301)	0.31 (0.41)	4.11 (4.11)	HOMO-2 $\rightarrow$ LUMO (+100%)
<b>11</b>	277 (278)	0.30 (0.46)	4.47 (4.45)	HOMO-2 $\rightarrow$ LUMO (+62%)
<b>12</b>	295 (299)	0.29 (0.38)	4.19 (4.14)	HOMO $\rightarrow$ LUMO+1 (+44%)

a) Values in parentheses are calculated in CH<sub>3</sub>CN solution. b) Only components with contribution greater than 44% are shown. Percentage contribution approximated by  $2 \times (c_i)^2 \times 100\%$ , where  $c_i$  is the coefficient for the particular orbital rotation.

1  
2  
3 Interestingly it turns out that the HE band, attributable mainly to the HOMO-2→LUMO  
4 transition for **7** and **9-11** (Table 4), and corresponding to a large transfer of electron density from  
5 the ferrocenylpyrazolic system to the aromatic ring (Figure 6 left as an example), involves a  
6 significant ICT process. Interestingly in chromophore **12** the major contribution to the HE band is  
7 the HOMO→LUMO+1 transition (Table 4), associated with a much less significant transfer of  
8 electronic density from the ferrocenyl and partially the pyrazolic system to the aromatic ring where  
9 the substituent is a strong electron donor, so as to prevent the ICT process (Figure 6 right).



21  
22  
23  
24  
25  
26  
27  
28  
29  
30  
31  
32  
33  
34  
35  
36  
37  
38  
39  
40  
41  
42  
43  
44 **Figure 6.** Isodensity plots of HOMO-2→LUMO and HOMO→LUMO+1 transitions mainly  
45 involved in the HE absorption band of chromophores **9** and **12** respectively calculated by the TD-  
46 DFT approach at B3LYP/6-31+G\*\* level.

## 51 52 Second-order Nonlinear Optical Properties

53  
54 The second order NLO responses of the molecular chromophores **1** and **7-12** were measured  
55 by the EFISH technique, which provides the  $\gamma_{\text{EFISH}}$  value, from which EFISH quadratic  
56 hyperpolarizability  $\beta_{\lambda}$  can be obtained through eq. 1<sup>17</sup>  
57  
58  
59  
60

$$\gamma_{EFISH} = (\mu\beta_{\lambda} / 5KT) + \gamma(-2\omega; \omega, \omega, 0) \quad (1)$$

where  $\mu$  is the ground state dipole moment,  $\mu\beta_{\lambda}/5kT$  the dipolar orientational contribution,  $\lambda$  is the fundamental wavelength of the incident photons in the EFISH experiment,  $\gamma(-2\omega; \omega, \omega, 0)$  is a third-order term at frequency  $\omega$  of the incident photons, corresponding to the cubic contribution to  $\gamma_{EFISH}$ , usually negligible for quite dipolar chromophores such as those studied in this work. Finally,  $\beta_{\lambda}$  is the projection along the dipole moment axis of the vectorial component  $\beta_{VEC}$  of the tensorial quadratic hyperpolarizability. In the following  $\beta_{\lambda}$  is reported as  $\beta_{1907}$  since the EFISH experiments were carried out working with a 1907 nm non-resonant incident wavelength. All the EFISH measurements were carried out in  $CHCl_3$  solutions at  $10^{-3}$  M concentration (see experimental). The experimental  $\mu\beta_{1907}$  values obtained for chromophores **1**, and **7-11** (each experimental value is the averages of 16 measurements) are reported in Table 5B, while the theoretical DFT values of the ground ( $\mu_g$ ) and first excited state ( $\mu_e$ ) dipole moments, together with the theoretical  $\beta$  and  $\mu\beta$  values calculated by the TD-DFT approach are reported in Table 5A. The  $\mu\beta_{1907}$  value of chromophore **12** was too small to be measured by the EFISH technique.

The experimental EFISH  $\mu\beta_{1907}$  value and, according to the two-level approximation,<sup>61, 62</sup> the theoretical quadratic hyperpolarizability  $\beta$  are positive for all the chromophores, being DFT calculated  $\Delta\mu$  values always positive and dependent upon the nature of the substituents in the *para* position of the aryl ring (Tables 5A and 5B), as expected for a ICT process involving a transfer of electronic density from the donor ferrocenyl pyrazole moiety to the aromatic ring (Figure 6) with an increase of the excited state dipole moment with respect to the ground state.

It turns out that according to the electron withdrawing strength of the substituent,  $\beta$  values between 7 and  $91 \times 10^{-30}$  esu have been calculated for chromophores **1** and **7-12**, with the higher values corresponding to **8**, carrying the  $NO_2$  group, to **9**, carrying the CN group, and to **10**, carrying the  $CF_3$  group, all with high or significant electron withdrawing properties (Table 5A). The

1  
2  
3 calculated values of  $\beta$  and  $\mu\beta$  of **8** are anomalously high if compared to the other chromophores  
4 (Table 5A), but in line with the anomalously high redshift of its HE absorption band and with the  
5  
6 (Table 5A), but in line with the anomalously high redshift of its HE absorption band and with the  
7  
8 much lower HOMO-LUMO gap. Evidence that the  $\beta$  value of chromophores **1** and **7-11** is  
9  
10 dominated by an ICT process, involving a significant electron transfer from the DD (donor-donor)  
11  
12 ferrocenylpyrazole moiety to the acceptor aromatic ring, is confirmed by the very low value  
13  
14 calculated for  $\beta$  of the DDD (donor-donor-donor) chromophore **12**, carrying the strong donor  
15  
16 dimethylamino group on the aryl ring (Table 5A).  
17  
18  
19  
20

21  
22 It must be pointed out that theoretical  $\beta$  and  $\mu\beta$  values of all the chromophores investigated  
23  
24 have been calculated by the TD-DFT approach using the less complete 6-31+G\*\* basis set, and the  
25  
26 B3LYP method (see Experimental) which cannot account in a satisfactory way the electron  
27  
28 correlation effects. Therefore, although both the B3LYP method and the basis set 6-31+G\*\* cannot  
29  
30 produce a satisfactory estimation of  $\beta$  values, they have been utilized in order to save computational  
31  
32 time when compared to inclusion of additional diffusion functions, which would require, for each  
33  
34 chromophore, the choice of an appropriate basis set for calculating a reliable  $\beta$  value. It follows that,  
35  
36 due to the above limitations, the calculated  $\beta$  values can give acceptable information on the general  
37  
38 trend (Tables 5A and 5B) for the series of chromophores **1** and **7-12**, but not on the absolute value  
39  
40 of  $\beta$  of each chromophore.  
41  
42  
43  
44  
45

46  
47 Despite this limitation, the expected trend between EFISH  $\mu\beta_{1907}$  and the theoretical  $\mu\beta$   
48  
49 values can be observed (Table 5A and 5B). We have thus calculated from  $\beta_{1907}$  values, by the two  
50  
51 levels approximation,<sup>61, 62</sup> taking as a reference of the energy of the first excited state of the HE  
52  
53 band, static  $\beta_0$  and consequently  $\mu\beta_0$  values corresponding to the zero incident wavelength (Table  
54  
55 5B) which should be better compared to TD-DFT calculated  $\mu\beta$  values. We have found thus that  
56  
57 absolute values of theoretical  $\mu\beta$  and experimental EFISH  $\mu\beta_{1907}$  or  $\mu\beta_0$  values of the various  
58  
59  
60

chromophores display an acceptable correlation, although not enough linear, reproduced in Figure 7.

**Table 5A.** Theoretical TD-DFT ground and first excited state dipole moments and values of  $\beta$  and  $\mu\beta$  for **1**, **7-12**.

Chromophore	$\mu_g^a$ (D)	$\mu_e^b$ (D)	$\Delta\mu^c$ (D)	$\mu\beta \times 10^{-48}$ (esu)	$\beta \times 10^{-30}$ (esu)
<b>1</b>	2.88	3.07	0.19	20.4	7.1
<b>7</b>	3.10	3.44	0.34	52.7	17
<b>8</b>	6.77	8.44	1.67	616	91
<b>9</b>	6.15	7.57	1.42	228	37
<b>10</b>	4.42	5.02	0.60	88.4	20
<b>11</b>	3.60	3.93	0.33	43.2	12
<b>12</b>	4.82	5.18	0.36	13.0	2.7

a)  $\mu_g$  = ground state dipole moment. b)  $\mu_e$  = excited state dipole moment. c)  $\Delta\mu$  = difference between excited and ground state dipole moment.

**Table 5B.** Experimental EFISH  $\mu\beta_{1907}$  and  $\mu\beta_0$  for **1**, **7-11**.

Chromophore	$\mu$ (D) <sup>a</sup>	$\mu\beta_{1907} \times 10^{-48}$ (esu)	$\mu\beta_0^b \times 10^{-48}$ (esu)
<b>1</b>	2.88	280	251
<b>7</b>	3.10	335	301
<b>8</b>	6.77	410	355
<b>9</b>	6.15	360	320
<b>10</b>	4.42	330	299
<b>11</b>	3.60	320	287
<b>12</b>	4.82	n.d. <sup>c</sup>	n.d. <sup>c</sup>

a) Theoretical DFT value of the ground state  $\mu_g$ ; b) static value calculated applying the two level approximation<sup>61, 62</sup> to EFISH  $\beta_{1907}$  taking as reference the energy of the first excited state of the HE band; c) too low value to be measured with an acceptable error.

Although such lack of linearity, mainly due to anomalously high  $\mu\beta_{1907}$  and  $\mu\beta$  values of **8**, it appears that the trend of the second order NLO response, experimentally measured as  $\mu\beta_{1907}$  or theoretical as  $\mu\beta$  is related, in a satisfactory way, to the  $\sigma$  values of the Hammett parameters<sup>63, 64</sup> of the substituents in para position of the aryl ring, which according to Ulman take into account both inductive and resonance effects.<sup>64</sup> In agreement with the larger red shift of both HE and ME electronic absorption bands of **8** and **9** with respect to **1**, due to a more significant ICT process, both theoretical  $\mu\beta$  and experimental  $\mu\beta_{1907}$  values are much higher for **8** and **9**, carrying stronger electron withdrawing groups with respect to other chromophores (Tables 5A and 5B)

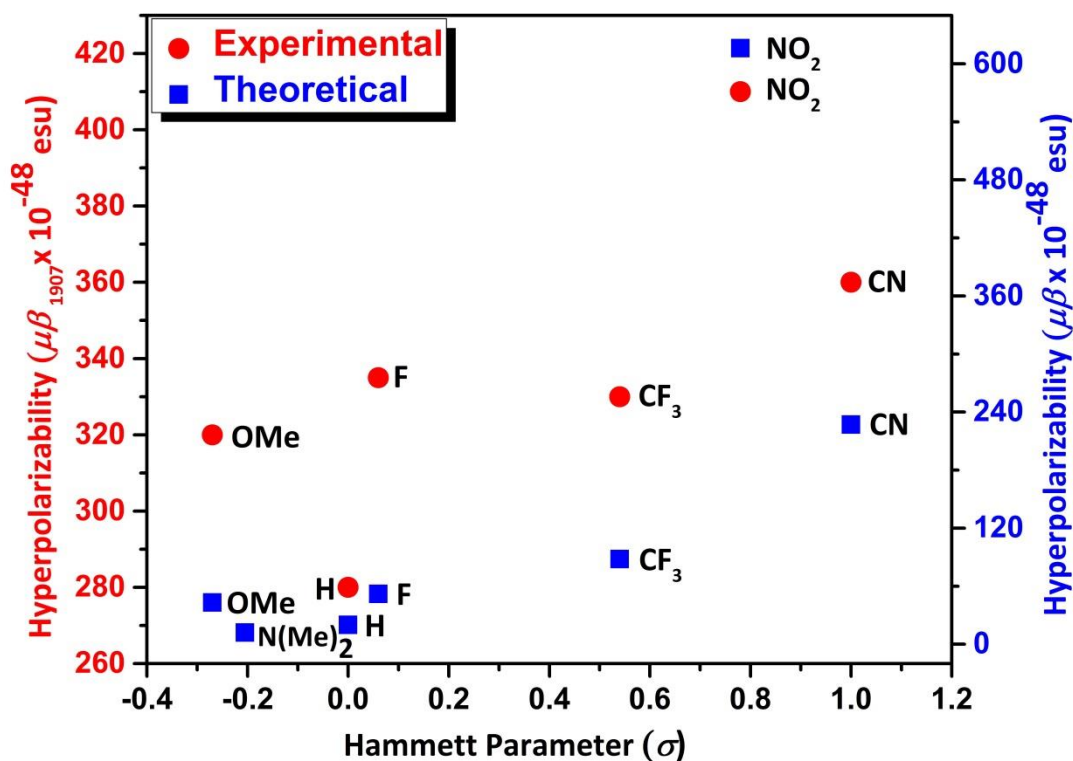


**Figure 7.** Correlation of the general trend of theoretical  $\mu\beta$  and experimental EFISH  $\mu\beta_{1907}$  values for chromophores **1** and **7-12** and their relation with respect to the electronic properties of substituents in para position of the aryl ring as defined by the Hammett parameters ( $\sigma$ ).

Finally, it is of interest to compare the magnitude of static  $\beta_0$  values of **1**, **7-11**, not dependent on the wavelength of the incident light, with static  $\beta_0$  values reported by Miller *et al.*<sup>39</sup> for a series of structurally related DA (donor-acceptor) ICT chromophores based on various N-arylpyrazoles, lacking the ferrocenyl moiety. In accordance with a more significant ICT process, DDA (donor-donor-acceptor) chromophores **1**, **7-11**, based on the ferrocenyl N-aryl pyrazole structure, show  $\beta_0$  values between 52.1 and 97.1  $\times 10^{-30}$  esu, much higher than those of the series of the structurally related DA chromophores, reported by Miller *et al.*,<sup>39</sup> which show  $\beta_0$  values between 4.6 and 30.7  $\times 10^{-30}$  esu.

## Conclusions

In this paper, we report on a series of new DDA chromophores based on the ferrocenyl N-aryl pyrazolic structure successfully synthesized using the Chan-Lam cross-coupling reaction between the appropriate arylboronic acid and the ferrocenyl pyrazole moiety. The chromophores **5**, **7**, **8** and **9**, fully characterized by single crystal X-ray diffraction, show a non-planar structure, confirmed by DFT calculations for all the chromophores. Electronic absorption spectra and TD-DFT theoretical investigation have produced evidence for a significant ICT process from the ferrocenyl system to the aryl ring. Despite the lack of planarity of the whole structure, the effects induced by the electronic properties of the substituents in the *para* position of the aryl ring are transmitted along the molecular structure to the ferrocenyl moiety. It follows that the features of electronic absorption spectra, electrochemical potentials and second order NLO responses of these new ICT chromophores are significantly tuned by the nature of the substituents in the *para* position of the aryl ring.

The second order NLO responses, theoretical  $\mu\beta$  and experimental  $\mu\beta_{1907}$ , increase with increasing the strength of the acceptor properties of the substituents, with anomalously high values in the case of  $\text{NO}_2$  substituent, and show a satisfactory relation of both  $\mu\beta$  and  $\mu\beta_{1907}$  with the Hammett  $\sigma$  parameters of the various substituents. The static  $\beta_0$  values of these new DDA ferrocenyl N-arylpyrazole chromophores, calculated by the two levels approximation,<sup>61, 62</sup> are much higher (between 52.1 and 97.1 x 10<sup>-30</sup> esu) than the  $\beta_0$  values reported by Miller et al.<sup>39</sup> for the related DA, N-arylpyrazoles lacking of the donor ferrocenyl moiety (between 4.6 and 30.7 x 10<sup>-30</sup> esu), thus showing that the connection between the of two strong donor moieties (ferrocene and pyrazole) can induce a significant increase of the second order NLO response of the ICT chromophores, producing  $\mu\beta_0$  values unexpectedly relevant (between 251 and 355 x 10<sup>-48</sup> esu).



1  
2  
3 In conclusion despite the lack of planarity of the whole  $\pi$  structure of these new ICT  
4 chromophores, the second order NLO response can be significantly tuned by the nature of the  
5 substituent on the aryl ring, and the DDA structural arrangement is the origin of a large increase of  
6 the second order nonlinear response. Moreover TD-DFT calculations clearly show that the  
7 pyrazolic part of the molecule does not act, as expected for a ICT process, as a simple  $\pi$  spacer  
8 between the donor ferrocenyl moiety and the acceptor aryl ring, as it occurs in classical  
9 intramolecular push-pull systems, but mainly as an additional  $\pi$  donor, which strengthens the donor  
10 properties of the ferrocenyl moiety thus favoring a very effective ICT process.  
11  
12  
13  
14  
15  
16  
17  
18  
19  
20  
21  
22  
23  
24  
25

## 26 **Experimental**

### 27 **Materials and Synthetic Procedures**

28  
29  
30  
31  
32  
33 The 3-Ferrocenyl-5-methyl-1H-pyrazole was synthesized according to the reported  
34 procedure.<sup>45</sup> Chromatographic purifications and separations were carried out using silica gel 60  
35 (AVRA, 100 – 120 mesh).  $\text{CH}_2\text{Cl}_2$  was distilled over  $\text{CaCl}_2$  prior to use. Other solvents were of  
36 reagent grade and were used without prior purification. All other chemicals were purchased from  
37 M/s. Aldrich Chemical Co. and M/s. Johnson Matthey Chemicals. Details on the general  
38 experimental conditions and on the analytical characterisation of chromophores are reported in the  
39 Supporting Information.  
40  
41  
42  
43  
44  
45  
46  
47  
48  
49

### 50 **General Physical Measurements**

51  
52  
53 The  $^1\text{NMR}$  spectra were recorded on a BRUKER (600 MHz) spectrometer. Chemical shifts  
54 are reported in  $\delta$  (ppm) and mass spectra were recorded on a GC-MS (PERKIN ELMER)  
55 spectrometer Infrared spectra were recorded on a PERKIN SHIMADZU spectrometer spectrum  
56 One as KBr diluted discs. Electronic absorption spectra were recorded using Agilent 8453 UV-  
57  
58  
59  
60

1  
2  
3 visible diode array spectrophotometer in CH<sub>3</sub>CN as a solvent. Electrochemical measurements were  
4  
5 performed in a 4 cm<sup>3</sup> cell, in 5 × 10<sup>-4</sup> - 10<sup>-3</sup> M solutions in acetonitrile (Aldrich, 99.8%) with 0.1 M  
6  
7 tetrabutylammonium perchlorate (TBAP, Aldrich) as the supporting electrolyte. The solutions were  
8  
9 de-aerated by N<sub>2</sub> bubbling. The ohmic drop has been compensated by the positive feedback  
10  
11 technique. The experiments were carried out using an AUTOLAB PGSTAT potentiostat  
12  
13 (EcoChemie, The Netherlands) run by a PC with GPES software. Cyclic voltammetry (CV)  
14  
15 investigations were carried out at scan rates typically ranging 0.05 to 2 Vs<sup>-1</sup>, with ohmic drop  
16  
17 compensation. The working electrode was a glassy carbon one (AMEL, diameter = 1.5 mm)  
18  
19 cleaned by synthetic diamond powder (Aldrich, diameter = 1 μm) with a wet cloth (STRUERS DP-  
20  
21 NAP); the counter electrode was a platinum wire. The operating reference electrode was an aqueous  
22  
23 saturated calomel electrode (SCE). To prevent water and chloride leakage into the working solution  
24  
25 a compartment filled with the operating medium and ending with a porous frit was interposed  
26  
27 between the reference electrode and the cell. Thermogravimetric analyses (TGA) were performed  
28  
29 (0-1000 °C) on a TGA SDT Q600 V20.9 Build 20 instrument under N<sub>2</sub> atmosphere, at a heating rate  
30  
31 of 20 °C min<sup>-1</sup>.  
32  
33  
34  
35  
36  
37  
38

### 39 **Single-crystal X-ray structural determination of chromophores 5, 7-9**

40  
41  
42 Crystals of **5**, **7-9** were obtained by a slow evaporation of the solutions (MeOH and DCM) at  
43  
44 room temperature. Crystals were stored in paraffin oil, mounted in a MiTeGenloop, and X-ray  
45  
46 diffraction measurements were done in the range 100 to 120 K. The crystal approximate dimensions  
47  
48 are 0.37 x 0.25 x 0.09 mm<sup>3</sup> (**5**), 0.35 x 0.23 x 0.17 mm<sup>3</sup> (**7**), 0.45 x 0.18 x 0.08 mm<sup>3</sup> (**8**) and 0.35 x  
49  
50 0.27 x 0.21 mm<sup>3</sup> (**9**). The X-ray diffraction data were collected on an Agilent SuperNova (Oxford  
51  
52 Diffraction) diffractometer using Mo-K<sub>α</sub> radiation (λ = 0.71073 Å). The Apex2<sup>65</sup> package was used  
53  
54 for cell refinements and data reductions. The structures were solved by direct methods using the  
55  
56 Shelxs 97<sup>66</sup> or Superflip<sup>67</sup> program with the Olex 2<sup>68</sup> graphical user interface. Structural refinements  
57  
58 were carried out using Shelxl-97 or Shelxl-2014.<sup>67, 69</sup>  
59  
60

1  
2  
3 The positions of all the atoms were obtained by direct methods. All non-hydrogen atoms  
4 were refined anisotropically. Hydrogen atoms were positioned geometrically and were also  
5  
6 constrained to ride on their parent atoms, with  $C - H = 0.95 \text{ \AA}$ , and  $U_{\text{iso}} = 1.2 U_{\text{eq}}$  (parent atom).  
7  
8  
9  
10 The crystallographic details are summarized in Table S1.  
11

### 12 13 **EFISH measurements**

14  
15  
16 All of the EFISH measurements<sup>70, 71</sup> were carried out in  $\text{CHCl}_3$  solutions at  $10^{-3} \text{ M}$   
17 concentration, working with a nonresonant incident wavelength of 1907 nm, using a Q-switched,  
18 mode-locked  $\text{Nd}^{3+}$ :YAG laser [pulse durations of 15 ns (90 ns) at a 10 Hz repetition rate]  
19 manufactured by Atalaser. The 1064 nm initial wavelength was shifted to 1907 nm by a Raman  
20 shifter with a high-pressure  $\text{H}_2$  cell. The apparatus for the EFISH measurements was made by  
21 SOPRA (France).  
22  
23  
24  
25  
26  
27  
28  
29  
30

31  
32 A high voltage was applied across the EFISH cell containing the solution. The EFISH cell  
33 consisted of a stainless steel container with two quartz optical windows that form a wedge-shaped  
34 cavity within the cell. The electrode was connected to the high voltage supply. The cell was  
35 mounted on an electrically isolated translation stage. The whole cell was then translated  
36 horizontally relative to the incident beam to produce fringes at the second harmonic wavelength.  
37  
38 Every measurement was referenced separately to the fringes of the pure solvent ( $\text{CHCl}_3$ ) that was  
39 used to dissolve the chromophore to consider laser power's fluctuations. The  $\mu\beta_{1907}$  values reported  
40 in Table 5B are the averages of 16 successive measurements performed on each sample. The  
41 standard deviation was never greater than 20%.  
42  
43  
44  
45  
46  
47  
48  
49  
50  
51  
52

### 53 54 **Theoretical Calculations**

55  
56  
57 The electronic structures and molecular properties of the ferrocenyl-N-pyrazolic  
58 chromophores investigated in this work were studied using the DFT (Density Functional Theory)  
59 method in order to define bonding patterns, electronic charge, and molecular orbital energy  
60

1  
2  
3 distributions, and the TD (Time Dependent)-DFT method to investigate the origin of electronic  
4  
5 absorption spectra and nonlinear optical properties. The initial geometry of chromophores was  
6  
7 taken from the available crystal data of **9** and guess structures of remaining chromophores were  
8  
9 obtained by changing the substituent in the *para* position of the aryl ring. The geometries of the  
10  
11 chromophores **1**, **7-12** in the gas phase were optimized using the Becke's three-parameter and Lee-  
12  
13 Yang-Parr functional (B3LYP).<sup>72</sup> The DFT calculations were carried out using the 6-31+G\*\* basis  
14  
15 set. On the optimized gas phase geometries, TD-DFT single point calculations have been carried out  
16  
17 at the B3LYP/6-31+G\*\* level, including the first 20 excited singlet states, both in the gas phase and  
18  
19 insolvent (CH<sub>3</sub>CN) phase using PCM (Polarizable Continuum Model) as solvation method. All  
20  
21 calculations were performed using the G09 package.<sup>73</sup> Electronic isodensity plots of frontier  
22  
23 molecular orbitals were obtained using GaussView 5<sup>74</sup> molecular visualization program.  
24  
25  
26  
27  
28  
29

## 30 **Acknowledgements**

31  
32  
33 KSK thanks to DST for Inspire fellowship (IF-110138). KSK and NP gratefully acknowledge SIF  
34  
35 DST-VIT-FIST, VIT University, Vellore for providing NMR, Mass and IR data. MP thanks, Prof.  
36  
37 Renato Ugo, Prof. Patrizia Mussini and Dr. Alessandra Forni for their extremely useful suggestions  
38  
39 and comments.  
40  
41  
42

## 43 **Supporting Information**

44  
45  
46 X-ray crystallographic data (1421536-1421538 (**5**, **7**, **9**) and 1428469 (**8**)) in CIF format and CIF  
47  
48 check and Cartesian coordinates, NMR, Mass, Cyclic Voltagram data. This material is available  
49  
50 free of charge via the Internet at <http://pubs.acs.org>.  
51  
52

## 53 **Author Information**

54  
55 Corresponding Authors

56  
57 \*E-mail: [palanisami.n@gmail.com](mailto:palanisami.n@gmail.com), [maddalena.pizzotti@unimi.it](mailto:maddalena.pizzotti@unimi.it)

58  
59 Notes  
60

The authors declare no competing financial interest.

## References

- 1  
2  
3  
4  
5  
6  
7 (1) Allard, S.; Forster, M.; Souharce, B.; Thiem, H.; Scherf, U. Organic Semiconductors for  
8 Solution-Processable Field-Effect Transistors (OFETs). *Angew. Chem. Int. Ed.* **2008**, *47*  
9 (22), 4070–4098.
- 10  
11 (2) Heck, J.; Dabek, S.; Meyer-Friedrichsen, T.; Wong, H. Mono- and Dinuclear  
12 Sesquifulvalene Complexes, Organometallic Materials with Large Nonlinear Optical  
13 Properties. *Coord. Chem. Rev.* **1999**, *190-192*, 1217–1254.
- 14  
15 (3) Clifford, J. N.; Martínez-Ferrero, E.; Viterisi, A.; Palomares, E. Sensitizer Molecular  
16 Structure-Device Efficiency Relationship in Dye Sensitized Solar Cells. *Chem. Soc. Rev.*  
17 **2011**, *40* (3), 1635–1646.
- 18  
19 (4) Wu, Y.; Zhu, W. Organic Sensitizers from D- $\pi$ -A to D-A- $\pi$ -A: Effect of the Internal  
20 Electron-Withdrawing Units on Molecular Absorption, Energy Levels and Photovoltaic  
21 Performances. *Chem. Soc. Rev.* **2013**, *42* (5), 2039–2058.
- 22  
23 (5) Joseph W. Perry. *Materials for Nonlinear Optics*; Marder, S. R., Sohn, J. E., Stucky, G. D.,  
24 Eds.; ACS Symposium Series; American Chemical Society: Washington, DC, 1991; Vol.  
25 455.
- 26  
27 (6) Twieg, R.; Azema, A.; Jain, K.; Cheng, Y. Y. Organic Materials for Non-Linear Optics  
28 Nitropyridine Derivatives. *Chem. Phys. Lett.* **1982**, *92* (2), 208–211.
- 29  
30 (7) Oudar, J. L.; Hierle, R. An Efficient Organic Crystal for Nonlinear Optics: Methyl- (2,4-  
31 Dinitrophenyl) -Aminopropanoate. *J. Appl. Phys.* **1977**, *48* (7), 2699.
- 32  
33 (8) Li, Y.; Liu, T.; Liu, H.; Tian, M.-Z.; Li, Y. Self-Assembly of Intramolecular Charge-  
34 Transfer Compounds into Functional Molecular Systems. *Acc. Chem. Res.* **2014**, *47* (4),  
35 1186–1198.
- 36  
37 (9) Zyss, J.; Ledoux, I. Nonlinear Optics in Multipolar Media: Theory and Experiments.  
38 *Chem. Rev.* **1994**, *94* (1), 77–105.
- 39  
40 (10) Verbiest, T.; Clays, K.; Samyn, C.; Wolff, J.; Reinhoudt, D.; Persoons, A. Investigations of  
41 the Hyperpolarizability in Organic Molecules from Dipolar to Octopolar Systems. *J. Am.*  
42 *Chem. Soc.* **1994**, *116* (20), 9320–9323.
- 43  
44 (11) Ledoux, I.; Zyss, J.; Siegel, J. S.; Brienne, J.; Lehn, J.-M. Second-Harmonic Generation  
45 from Non-Dipolar Non-Centrosymmetric Aromatic Charge-Transfer Molecules. *Chem.*  
46 *Phys. Lett.* **1990**, *172* (6), 440–444.
- 47  
48 (12) Barlow, S.; Marder, S. R. Electronic and Optical Properties of Conjugated Group 8  
49 Metallocene Derivatives. *Chem. Commun.* **2000**, No. 17, 1555–1562.
- 50  
51 (13) Blackburn, O. A.; Coe, B. J.; Helliwell, M. Tetrapalladium(II) Bisazobenzene and  
52 Azoazoxybenzene Complexes: Syntheses, Electronic Structures, and Optical Properties.  
53 *Organometallics* **2011**, *30* (18), 4910–4923.
- 54  
55 (14) Calabrese, J. C.; Cheng, L. T.; Green, J. C.; Marder, S. R.; Tam, W. Molecular Second-  
56 Order Optical Nonlinearities of Metallocenes. *J. Am. Chem. Soc.* **1991**, *113* (19), 7227–  
57 7232.
- 58  
59 (15) Green, M. L. H.; Marder, S. R.; Thompson, M. E.; Bandy, J. A.; Bloor, D.; Kolinsky, P.  
60 V.; Jones, R. J. Synthesis and Structure of (Cis)-[1-Ferrocenyl-2-(4-Nitrophenyl)ethylene],

- an Organotransition Metal Compound with a Large Second-Order Optical Nonlinearity. *Nature* **1987**, *330* (6146), 360–362.
- (16) Coe, B. J. Developing Iron and Ruthenium Complexes for Potential Nonlinear Optical Applications. *Coord. Chem. Rev.* **2013**, *257* (9-10), 1438–1458.
- (17) Bella, S. Di; Dragonetti, C.; Pizzotti, M.; Roberto, D.; Tessore, F.; Ugo, R. *Molecular Organometallic Materials for Optics*; Bozec, H., Guerchais, V., Eds.; Topics in Organometallic Chemistry; Springer Berlin Heidelberg: Berlin, Heidelberg, 2010; Vol. 28.
- (18) Woodward, R. B.; Rosenblum, M.; Whiting, M. C. A New Aromatic System. *J. Am. Chem. Soc.* **1952**, *74* (13), 3458–3459.
- (19) Barlow, S.; O'Hare, D. Metal–Metal Interactions in Linked Metallocenes. *Chem. Rev.* **1997**, *97* (3), 637–670.
- (20) Miller, J. S.; Epstein, A. J. Organic and Organometallic Molecular Magnetic Materials—Designer Magnets. *Angew. Chem. Int. Ed.* **1994**, *33* (4), 385–415.
- (21) Ratera, I.; Sporer, C.; Ruiz-Molina, D.; Ventosa, N.; Baggerman, J.; Brouwer, A. M.; Rovira, C.; Veciana, J. Solvent Tuning from Normal to Inverted Marcus Region of Intramolecular Electron Transfer in Ferrocene-Based Organic Radicals. *J. Am. Chem. Soc.* **2007**, *129* (19), 6117–6129.
- (22) Beer, P. D. Transition-Metal Receptor Systems for the Selective Recognition and Sensing of Anionic Guest Species. *Acc. Chem. Res.* **1998**, *31* (2), 71–80.
- (23) Mata, J. A.; Peris, E.; Asselberghs, I.; Van Boxel, R.; Persoons, A. Large Second-Order NLO Properties of New Conjugated Oligomers with a Pendant Ferrocenyl and an End-Capped Pyridine. *New J. Chem.* **2001**, *25* (8), 1043–1046.
- (24) Barlow, S.; Bunting, H. E.; Ringham, C.; Green, J. C.; Bublitz, G. U.; Boxer, S. G.; Perry, J. W.; Marder, S. R. Studies of the Electronic Structure of Metallocene-Based Second-Order Nonlinear Optical Dyes. *J. Am. Chem. Soc.* **1999**, *121* (15), 3715–3723.
- (25) Senthilkumar, K.; Thirumoorthy, K.; Dragonetti, C.; Marinotto, D.; Righetto, S.; Colombo, A.; Haukka, M.; Palanisami, N. Ferrocene–quinoxaline Y-Shaped Chromophores as Fascinating Second-Order NLO Building Blocks for Long Lasting Highly Active SHG Polymeric Films. *Dalt. Trans.* **2016**, *45* (30), 11939–11943.
- (26) Wang, W.-Y.; Ma, N.-N.; Sun, S.-L.; Qiu, Y.-Q. Impact of Redox Stimuli on Ferrocene–Buckybowl Complexes: Switchable Optoelectronic and Nonlinear Optical Properties. *Organometallics* **2014**, *33* (13), 3341–3352.
- (27) Wang, W.-Y.; Wang, L.; Ma, N.-N.; Zhu, C.-L.; Qiu, Y.-Q. Ferrocene/fullerene Hybrids Showing Large Second-Order Nonlinear Optical Activities: Impact of the Cage Unit Size. *Dalt. Trans.* **2015**, *44* (21), 10078–10088.
- (28) Wang, W.-Y.; Ma, N.-N.; Sun, S.-L.; Qiu, Y.-Q. Redox Control of Ferrocene-Based Complexes with Systematically Extended  $\pi$ -Conjugated Connectors: Switchable and Tailorable Second Order Nonlinear Optics. *Phys. Chem. Chem. Phys.* **2014**, *16* (10), 4900–4910.
- (29) Wang, W.-Y.; Ma, N.-N.; Wang, L.; Zhu, C.-L.; Fang, X.-Y.; Qiu, Y.-Q. Effect of  $\pi$ -Conjugate Units on the Ferrocene-Based Complexes: Switchable Second Order Nonlinear Optics Controlled by Redox Stimuli. *Dye. Pigment.* **2016**, *126*, 29–37.
- (30) Hitz, C. B.; Ewing, J.; Hecht, J. *Introduction to Laser Technology*; John Wiley & Sons, Inc.: Hoboken, NJ, USA, 2012.

- 1  
2  
3  
4  
5  
6  
7  
8  
9  
10  
11  
12  
13  
14  
15  
16  
17  
18  
19  
20  
21  
22  
23  
24  
25  
26  
27  
28  
29  
30  
31  
32  
33  
34  
35  
36  
37  
38  
39  
40  
41  
42  
43  
44  
45  
46  
47  
48  
49  
50  
51  
52  
53  
54  
55  
56  
57  
58  
59  
60
- (31) Jin, M.; Liang, Y. J.; Lu, R.; Chuai, X. H.; Yi, Z. H.; Zhao, Y.; Zhang, H. J. Synthesis and Properties of Photoluminescence and Electroluminescence of Pyrazoline Derivatives. *Synth. Met.* **2004**, *140* (1), 37–41.
- (32) Bian, B.; Ji, S.-J.; Shi, H.-B. Synthesis and Fluorescent Property of Some Novel Bichromophore Compounds Containing Pyrazoline and Naphthalimide Groups. *Dye. Pigment.* **2008**, *76* (2), 348–352.
- (33) Szukalski, A.; Sznitko, L.; Cyprych, K.; Miniewicz, A.; Mysliwiec, J. Light Amplification in Derivatives of Pyrazoline-Based Systems. *J. Phys. Chem. C* **2014**, *118* (15), 8102–8110.
- (34) Cyprych, K.; Sznitko, L.; Morawski, O.; Miniewicz, A.; Rau, I.; Mysliwiec, J. Spontaneous Crystallization and Aggregation of DCNP Pyrazoline-Based Organic Dye as a Way to Tailor Random Lasers. *J. Phys. D. Appl. Phys.* **2015**, *48* (19), 195101.
- (35) Manea, A.-M.; Rau, I.; Tane, A.; Kajzar, F.; Sznitko, L.; Miniewicz, A. Poling Kinetics and Second Order NLO Properties of DCNP Doped PMMA Based Thin Film. *Opt. Mater. (Amst.)* **2013**, *36* (1), 69–74.
- (36) Papagiannouli, I.; Szukalski, a.; Iliopoulos, K.; Mysliwiec, J.; Couris, S.; Sahraoui, B. Pyrazoline Derivatives with a Tailored Third Order Nonlinear Optical Response. *RSC Adv.* **2015**, *5* (60), 48363–48367.
- (37) Makowska-Janusik, M.; Kajzar, F.; Miniewicz, A.; Mydlova, L.; Rau, I. First Principle Calculations of the Electronic and Vibrational Properties of the 3-(1,1-Dicyanoethenyl)-1-Phenyl-4,5-Dihydro-1H-Pyrazole Molecule. *J. Phys. Chem. A* **2015**, *119* (8), 1347–1358.
- (38) Mukherjee, S.; Salini, P. S.; Srinivasan, A.; Peruncheralathan, S. AIEE Phenomenon: Tetraaryl vs. Triaryl Pyrazoles. *Chem. Commun.* **2015**, *51* (96), 17148–17151.
- (39) Miller, R. D.; Moylan, C. R.; Reiser, O.; Walsh, C. a. Heterocyclic Azole Nonlinear Optical Chromophores. 1. Donor-Acceptor Substituted Pyrazole Derivatives. *Chem. Mater.* **1993**, *5* (14), 625–632.
- (40) Dwivedi, Y.; de Boni, L.; Gonçalves, P. J.; Mairink, L. M.; Menegatti, R.; Fonseca, T. L.; Zilio, S. C. Experimental and Theoretical Investigation of Optical Nonlinearities in (Nitrovinyl)-1H-Pyrazole Derivative. *Spectrochim. Acta. A. Mol. Biomol. Spectrosc.* **2013**, *105*, 483–487.
- (41) Moylan, C. R.; Twieg, R. J.; Lee, V. Y.; Swanson, S. A.; Betterton, K. M.; Miller, R. D. Nonlinear Optical Chromophores with Large Hyperpolarizabilities and Enhanced Thermal Stabilities. *J. Am. Chem. Soc.* **1993**, *115* (26), 12599–12600.
- (42) Moylan, C. R.; Miller, R. D.; Twieg, R. J.; Betterton, K. M.; Lee, V. Y.; Matray, T. J.; Nguyen, C. Synthesis and Nonlinear Optical Properties of Donor-Acceptor Substituted Triaryl Azole Derivatives. *Chem. Mater.* **1993**, *5* (10), 1499–1508.
- (43) Lam, P. Y. .; Clark, C. G.; Saubern, S.; Adams, J.; Winters, M. P.; Chan, D. M. .; Combs, A. New Aryl/heteroaryl C-N Bond Cross-Coupling Reactions via Arylboronic Acid/cupric Acetate Arylation. *Tetrahedron Lett.* **1998**, *39* (19), 2941–2944.
- (44) Chan, D. M. .; Monaco, K. L.; Wang, R.-P.; Winters, M. P. New N- and O-Arylations with Phenylboronic Acids and Cupric Acetate. *Tetrahedron Lett.* **1998**, *39* (19), 2933–2936.
- (45) Sergeev, E. E.; Fabinskii, P. V.; Fedorov, V. A.; Korol'kova, I. V.; Kulebakin, V. G. Synthesis and Physicochemical Properties of Crystalline Tris(ferrocenoyl)acetate Hydrates of Some Rare-Earth Elements. *Russ. J. Coord. Chem.* **2008**, *34* (5), 382–387.

- 1  
2  
3 (46) Shi, Y.-C.; Zhu, B.-B.; Sui, C.-X. -Pyrazole. *Acta Crystallogr. Sect. E Struct. Reports*  
4 *Online* **2006**, 62 (9), m2389–m2391.
- 5  
6 (47) Wanniarachchi, S.; Liddle, B. J.; Lindeman, S. V.; Gardinier, J. R. Preparation, Properties,  
7 and Reactivity of carbonylrhodium(I) Complexes of di(2-Pyrazolylaryl)amido-Pincer  
8 Ligands. *J. Organomet. Chem.* **2011**, 696 (23), 3623–3636.
- 9  
10 (48) Lambert, C.; Wagener, R.; Klein, J. H.; Grelaud, G.; Moos, M.; Schmiedel, A.; Holzapfel,  
11 M.; Bruhn, T. A Photoinduced Mixed-Valence State in an Organic Bis-Triarylamine  
12 Mixed-Valence Compound with an Iridium-Metal-Bridge. *Chem. Commun.* **2014**, 50 (77),  
13 11350-11353.
- 14  
15 (49) Kaddouri, H.; Vicente, V.; Ouali, A.; Ouazzani, F.; Taillefer, M. Copper-Catalyzed  
16 Arylation of Nucleophiles by Using Butadienylphosphines as Ligands: Mechanistic  
17 Insight. *Angew. Chem. Int. Ed.* **2009**, 48 (2), 333–336.
- 18  
19 (50) Chevallier, F.; Halauko, Y. S.; Pecceu, C.; Nassar, I. F.; Dam, T. U.; Roisnel, T.; Matulis,  
20 V. E.; Ivashkevich, O. a.; Mongin, F. N-Aryl Pyrazoles: DFT Calculations of CH Acidity  
21 and Deprotonative Metallation Using a Combination of Lithium and Zinc Amides. *Org.*  
22 *Biomol. Chem.* **2011**, 9 (12), 4671-4684.
- 23  
24 (51) Coe, B. J.; Docherty, R. J.; Foxon, S. P.; Harper, E. C.; Helliwell, M.; Raftery, J.; Clays,  
25 K.; Franz, E.; Brunshwig, B. S. Syntheses and Properties of Salts of Chromophores with  
26 Ferrocenyl Electron Donor Groups and Quaternary Nitrogen Acceptors. *Organometallics*  
27 **2009**, 28 (24), 6880–6892.
- 28  
29 (52) Kaur, P.; Kaur, M.; Depotter, G.; Van Cleuvenbergen, S.; Asselberghs, I.; Clays, K.;  
30 Singh, K. Thermally Stable Ferrocenyl “push–pull” Chromophores with Tailorable and  
31 Switchable Second-Order Non-Linear Optical Response: Synthesis and Structure–property  
32 Relationship. *J. Mater. Chem.* **2012**, 22 (21), 10597-10608.
- 33  
34 (53) Jacquemin, D.; Femenias, A.; Chermette, H.; André, J.-M.; Perpète, E. A. Second-Order  
35 Møller–Plesset Evaluation of the Bond Length Alternation of Several Series of Linear  
36 Oligomers. *J. Phys. Chem. A* **2005**, 109 (25), 5734–5741.
- 37  
38 (54) Dehu, C.; Meyers, F.; Bredas, J. L. Donor-Acceptor Diphenylacetylenes: Geometric  
39 Structure, Electronic Structure, and Second-Order Nonlinear Optical Properties. *J. Am.*  
40 *Chem. Soc.* **1993**, 115 (14), 6198–6206.
- 41  
42 (55) Venkatraman, S.; Kumar, R.; Sankar, J.; Chandrashekar, T. K.; Sendhil, K.; Vijayan, C.;  
43 Kelling, A.; Senge, M. O. Oxasmaragdyrin–Ferrocene and Oxacorrole–Ferrocene  
44 Conjugates: Synthesis, Structure, and Nonlinear Optical Properties. *Chem. Eur. J.* **2004**, 10  
45 (6), 1423–1432.
- 46  
47 (56) Kaur, S.; Dhoun, S.; Depotter, G.; Kaur, P.; Clays, K.; Singh, K. Synthesis, Linear and  
48 Nonlinear Optical Properties of Thermally Stable Ferrocene-Diketopyrrolopyrrole Dyads.  
49 *RSC Adv.* **2015**, 5 (103), 84643–84656.
- 50  
51 (57) Connelly, N. G.; Geiger, W. E. Chemical Redox Agents for Organometallic Chemistry.  
52 *Chem. Rev.* **1996**, 96 (2), 877–910.
- 53  
54 (58) Misra, R.; Gautam, P.; Mobin, S. M. Aryl-Substituted Unsymmetrical Benzothiadiazoles:  
55 Synthesis, Structure, and Properties. *J. Org. Chem.* **2013**, 78 (24), 12440–12452.
- 56  
57 (59) Burnes, D. M.  $\beta$ -Keto Acetals. I. Synthesis of Pyrazoles and Pyrimidines and the Steric  
58 Inhibition of Resonance in 5-Alkyl-1- P -Nitrophenylpyrazoles. *J. Org. Chem.* **1956**, 21  
59 (1), 97–101.
- 60



- 1  
2  
3  
4  
5  
6  
7  
8  
9  
10  
11  
12  
13  
14  
15  
16  
17  
18  
19  
20  
21  
22  
23  
24  
25  
26  
27  
28  
29  
30  
31  
32  
33  
34  
35  
36  
37  
38  
39  
40  
41  
42  
43  
44  
45  
46  
47  
48  
49  
50  
51  
52  
53  
54  
55  
56  
57  
58  
59  
60
- (60) Rabie, U. M. Intra- and Intermolecular Charge Transfer: Twin Themes and Simultaneous Competing Transitions Involving Ferrocenes. *Spectrochim. Acta Part A Mol. Biomol. Spectrosc.* **2009**, *74* (3), 746–752.
- (61) Oudar, J. L. Optical Nonlinearities of Conjugated Molecules. Stilbene Derivatives and Highly Polar Aromatic Compounds. *J. Chem. Phys.* **1977**, *67* (2), 446-457.
- (62) Oudar, J. L.; Chemla, D. S. Hyperpolarizabilities of the Nitroanilines and Their Relations to the Excited State Dipole Moment. *J. Chem. Phys.* **1977**, *66* (6), 2664-2668.
- (63) Park, G.; Cho, B. R. First Hyperpolarizabilities of Triazine derivatives. Ab Initio Studies and Hammett Correlation. *J. Phys. Org. Chem.* **2004**, *17* (3), 169–173.
- (64) Park, G.; Cho, B. R. First Hyperpolarizabilities of 1,3,5-Tricyano-2,4,6-Tris(styryl)benzene Derivatives: ab Initio Studies and Hammett Correlation. *J. Phys. Org. Chem.* **2005**, *18* (3), 264–267.
- (65) Bruker, A. X. S. “APEX2-Software Suite for Crystallographic Programs.” Bruker AXS Inc., Madison. Bruker AXS, Inc., Madison, WI, USA 2009.
- (66) Sheldrick, G. M. A Short History of SHELX. *Acta Crystallogr. Sect. A* **2008**, *64* (1), 112–122.
- (67) Palatinus, L.; Chapuis, G. SUPERFLIP – a Computer Program for the Solution of Crystal Structures by Charge Flipping in Arbitrary Dimensions. *J. Appl. Crystallogr.* **2007**, *40* (4), 786–790.
- (68) Dolomanov, O. V.; Bourhis, L. J.; Gildea, R. J.; Howard, J. a K.; Puschmann, H. OLEX2: A Complete Structure Solution, Refinement and Analysis Program. *J. Appl. Crystallogr.* **2009**, *42* (2), 339–341.
- (69) G. M. Sheldrick, SHELXTL, Bruker AXS, Inc., Madison, Wisconsin, USA. 2008.
- (70) Ledoux, I.; Zyss, J. Influence of the Molecular Environment in Solution Measurements of the Second-Order Optical Susceptibility for Urea and Derivatives. *Chem. Phys.* **1982**, *73* (1-2), 203–213.
- (71) Singer, K. D. Measurements of Molecular Second Order Optical Susceptibilities Using Dc Induced Second Harmonic Generation. *J. Chem. Phys.* **1981**, *75* (7), 3572-3580.
- (72) Lee, C.; Yang, W.; Parr, R. G. Development of the Colle-Salvetti Correlation-Energy Formula into a Functional of the Electron Density. *Phys. Rev. B* **1988**, *37* (2), 785–789.
- (73) Frisch, M. J.; Trucks, G. W.; Schlegel, H. B.; Scuseria, G. E.; Robb, M. A.; Cheeseman, J. R.; Scalmani, G.; Barone, V.; Mennucci, B.; Petersson, G. A.; Nakatsuji, H.; Caricato, M.; Li, X.; Hratchian, H. P.; Izmaylov, A. F.; Bloino, J.; Zheng, G.; Sonnenb, D. J. Gaussian, Inc., Wallingford, CT, **2009**.
- (74) Dennington, Roy; Keith, Todd; Millam, J. GaussView, Version 5.0.9. Semichem Inc., KS 2009.

## TOC Graphic

